AFRL-RX-WP-TP-2012-0251

THERMAL MECHANICAL FATIGUE CRACKS GROWTH FROM LASER DRILLED HOLES IN SINGLE CRYSTAL MATERIAL (PREPRINT)

R.K. Kersey and A. Staroselsky
Pratt & Whitney

D.C. Dudzinski and M. Genest
National Research Council Canada, Institute for Aerospace Research

MARCH 2012

AIR FORCE RESEARCH LABORATORY
MATERIALS AND MANUFACTURING DIRECTORATE
WRIGHT-PATTERSON AIR FORCE BASE, OH 45433-7750
AIR FORCE MATERIEL COMMAND
UNITED STATES AIR FORCE

REPORT DOCUMENTATION PAGE

Form Approved
OMB No. 0704-0188

1. REPORT DATE *(DD-MM-YY)*	2. REPORT TYPE	3. DATES COVERED *(From - To)*
March 2012	Technical Paper	1 March 2012 – 1 March 2012

4. TITLE AND SUBTITLE
THERMAL MECHANICAL FATIGUE CRACKS GROWTH FROM LASER DRILLED HOLES IN SINGLE CRYSTAL MATERIAL (PREPRINT)

5a. CONTRACT NUMBER
FA8650-07-C-5252

5b. GRANT NUMBER

5c. PROGRAM ELEMENT NUMBER
62102F

6. AUTHOR(S)
R.K. Kersey and A. Staroselsky (Pratt & Whitney)
D.C. Dudzinski and M. Genest (National Research Council Canada, Institute for Aerospace Research)

5d. PROJECT NUMBER
4347

5e. TASK NUMBER
20

5f. WORK UNIT NUMBER
24110202

7. PERFORMING ORGANIZATION NAME(S) AND ADDRESS(ES)
Pratt & Whitney
400 Main Street
E. Hartford, CT 06108-0968

8. PERFORMING ORGANIZATION REPORT NUMBER
AFRL-RX-WP-TP-2012-0251

9. SPONSORING/MONITORING AGENCY NAME(S) AND ADDRESS(ES)
Air Force Research Laboratory
Materials and Manufacturing Directorate
Wright-Patterson Air Force Base, OH 45433-7750
Air Force Materiel Command
United States Air Force

10. SPONSORING/MONITORING AGENCY ACRONYM(S)
AFRL/RXLM

11. SPONSORING/MONITORING AGENCY REPORT NUMBER(S)
AFRL-RX-WP-TP-2012-0251

12. DISTRIBUTION/AVAILABILITY STATEMENT
Approved for public release; distribution unlimited.

13. SUPPLEMENTARY NOTES
The U.S. Government is joint author of this work and has the right to use, modify, reproduce, release, perform, display, or disclose the work. PA Case Number and clearance date: 88ABW-2012-0444, 30 Jan 2012. Postprint journal was submitted to Experimental Mechanics. This document contains color.

14. ABSTRACT
The crack growth test results undergoing thermomechanical fatigue showed that the life of TMF specimens with notched laser drilled holes exhibit a debit by as much as 4 times that of smooth gage section specimens under the same loading conditions. Such a significant change in number of cycles to failure must be accounted in any damage tolerant design system. The detailed fractographic analysis demonstrated that the all cracks start crystallographically along the <111> octahedral crystallographic planes and later change to mixed mode fracture. Major crack propagation takes place at the low temperature portion of the cycle in the OP test; however there is noticeable damage accumulation during the high temperature compressive load portion of the cycle. Crack propagation under TMF loading conditions is considerably faster than corresponding isothermal LCF crack growth tested at the temperature and similar loading conditions of the tensile part of the TMF cycle. As results show, the applicability of the LEFM methods for single crystal TMF crack growth prediction is limited and at least should consist of mixed mode crack analysis.

15. SUBJECT TERMS
thermomechanical fatigue, cooled turbine blade, fatigue crack growth, single crystal superalloy

16. SECURITY CLASSIFICATION OF:			17. LIMITATION OF ABSTRACT:	NUMBER OF PAGES	19a. NAME OF RESPONSIBLE PERSON (Monitor)
a. REPORT	b. ABSTRACT	c. THIS PAGE			Andrew Rosenberger
Unclassified	Unclassified	Unclassified	SAR	24	19b. TELEPHONE NUMBER *(Include Area Code)* N/A

Thermal Mechanical Fatigue Cracks Growth from Laser Drilled Holes in Single Crystal Material

R. K. Kersey[1], A. Staroselsky[1], D. C. Dudzinski[2], and M. Genest[2].

[1] Pratt & Whitney, East Hartford CT, USA 06108

[2] National Research Council Canada, Institute for Aerospace Research, 1200 Montreal Rd, Ottawa, ON, Canada K1A 0R6

Abstract

The crack growth test results undergoing thermomechanical fatigue showed that the life of TMF specimens with notched laser drilled holes exhibit a debit by as much as 4 times that of smooth gage section specimens under the same loading conditions. Such a significant change in number of cycles to failure must be accounted in any damage tolerant design system. The detailed fractographic analysis demonstrated that the all cracks start crystallographically along the <111> octahedral crystallographic planes and later change to mixed mode fracture. Major crack propagation takes place at the low temperature portion of the cycle in the OP test; however there is noticeable damage accumulation during the high temperature compressive load portion of the cycle. Crack propagation under TMF loading conditions is considerably faster than corresponding isothermal LCF crack growth tested at the temperature and similar loading conditions of the tensile part of the TMF cycle. As results show, the applicability of the LEFM methods for single crystal TMF crack growth prediction is limited and at least should consist of mixed mode crack analysis.

A new method for detecting cracks during a TMF test using induction thermography was employed. This method, coined the Active Inferred Crack Detection System (AICD), demonstrated high effectiveness in following crack progression under cyclic loading making it well suited to perform TMF crack growth testing**.** Using this experimental technique we also investigated the effect of secondary crystallographic orientation on crack propagation by drilling 2 crack emanating holes 135° degrees apart from one another.

1. Introduction

Turbines in aircraft turbojet engines are being subject to increasingly higher temperatures to improve fuel efficiency. High turbine efficiency requires the ability of turbine blades to withstand gas temperature of the order of 1350 -1550 degrees centigrade. In polycrystalline materials these increased temperatures would cause creep strains along grain boundaries that would be unacceptable. Turbine blades must maintain adequate strength throughout long service intervals for commercial engines and throughout many complex mission types for military engines. Even single crystal materials though must be pushed to their limits to insure that engine performance is maximized. Airfoils in modern gas turbine aircraft use a systems approach for cooling to achieve required component life. There are three basic components to these systems: (i) a cast nickel single crystal super alloy in combination with (ii) thermal barrier coatings and finally a sophisticated (iii) cooling scheme consisting of intricately designed channels and holes through the core and surface of the airfoil.

A typical modern single crystal superalloy has the ordered $L1_2$ structure, with a matrix based on a γ face-centered cubic structure and regular cubes of γ' phase, based on the intermetallic compound Ni_3Al, which occupy from 65 to 70% of the volume [1]. The composition of these superalloys has evolved parallel with advancements in investment casting processes. Single crystal alloys are precipitation-strengthened, cast, mono-grain superalloys based on the Nickel-Chromium-Aluminum (Ni-Cr-Al) system [2]. The macrostructure is characterized by parallel continuous primary dendrites spanning the casting without interruption in the direction of solidification. A typical microstructure of the second generation Ni-base superalloy is shown in Fig. 1.

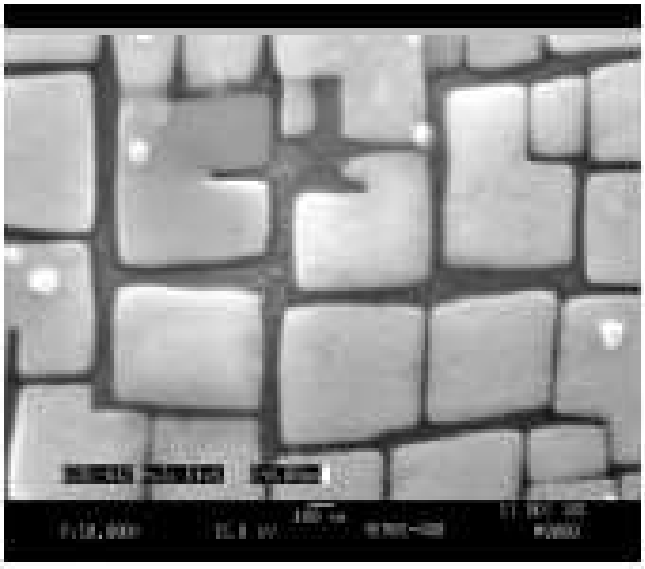

Figure 1. Typical microstructure of Ni-based superalloy single crystal PWA 1484.

The excellent high-temperature creep and fatigue resistance of these superalloys is a result of a combination of solid-solution strengthening, absence of deleterious grain boundaries, and a high volume fraction of precipitates that act as barriers to dislocation

motion [3]. However, fatigue crack initiation also depends on the microscopic defects, which can be categorized as intrinsic defects and deviant material defects.

Single superalloy crystals deform at high temperature by shearing along twelve octahedral {111}<110> and six cube {001}<110> slip systems. TMF cracking is usually taken place when inelastic deformation and corresponding energy dissipation is suppressed at low temperatures while creep and oxidation occur at high temperatures and generate stress redistribution affecting low temperature state. Recently, MacLachlan and Knowles [4], Staroselsky and Cassenti [5, 6] used a slip system model and structural elasto-viscoplastic calculation procedures for analysis of turbine components. Critical locations in turbine airfoils are subject to the combined influences of thermally driven strain transients and creep damage resulting from stresses during operation [7]. TMF cracking occurs at many locations on turbine airfoils, including pressure and suction sides and both leading and trailing edges [8, 9]. In single crystal blades, cracks are observed both parallel and normal to the casting growth direction. There is considerable blade-to-blade variation in the region where fatigue cracks are initiated at the cooling holes because of geometry properties and BC variations. The phasing between thermal and mechanical loads defines the TMF response of the airfoil [7-11]. The extremes of load-temperature phasing are in-phase (IP) and out-of-phase (OP). In-phase cycles occur when an unconstrained local area of the blade is mechanically loaded at the same time the temperature increases. Out-of-phase cycling occurs when a locally constrained area of the blade tries to expand both mechanically and thermally as temperature increases, which usually causes the local compression with the rise of temperature. OP cycling is generally the most harmful because stress relaxation at the maximum temperature develops high mean stresses.

Hot section components in advanced gas turbine engines experience severe cyclic temperature gradients and mechanical loads, particularly during takeoff and landing operations. As a consequence, thermal mechanical fatigue (TMF) is a major life-limiting factor for cooled gas turbine blades. TMF cracks are nucleated at the blade leading edge cooling hole locations due to a combination of high mechanical and thermal cyclic stresses and strains [9, 12]. The synergy between fatigue damage and time-dependent phenomena, such as creep and oxidation, can be much stronger under thermal transient conditions than under isothermal loading conditions [13, 14]. Therefore, TMF testing is extremely important in order to simulate the deformation and cracking behavior of blades at performance-critical locations [12-17].

While actual turbine blade TMF cycles are a combination of in-phase and out-of-phase cycles, two basic types of TMF cycles are commonly employed in laboratories: IP cycle, where the mechanical strain is the highest at the maximum temperature, and OP cycle, where the mechanical strain is the highest at the minimum temperature. It is, of course, possible to use any arbitrary phase angle between the specimen temperature and mechanical strain. While temperature varies periodically with time, special care is exercised to minimize the temperature gradient across the specimen section. This requirement for spatial uniformity in dynamic temperature distribution within the gage section necessitates relatively long cycle times. TMF testing requires careful monitoring, control, and measurement of a large number of experimental variables. The test data obtained on smooth specimens is traditionally used for the design purposes. As a result,

only safety-based design approaches might be employed. However, for the damage tolerant assessment, it is essential, if not critical that TMF crack initiation, location, propagation path, and growth rate information are developed as well. The development of methodology for a TMF damage-tolerant approach based on fracture mechanics is needed in order to reveal these specific physical damage phenomena. In addition, any fracture mechanics TMF modeling is required test data on TMF crack growth mechanisms and kinetics.

As have been already noted, most TMF cracks in airfoils start from the cooling holes. Thus, a new thermal fatigue experimental technique is needed to measure the structural life of the specimen containing through holes similar to the ones that are drilled in a cooled airfoils. In this paper we describe our basic TMF test procedure on specimens with laser drilled holes. We investigate the cooling holes effect on intrinsic serviceable fatigue crack growth and on corresponding TMF life compared to base line cast nickel single crystal data. The developed method would allow explicit measurements of the effects of crystal secondary orientation, holes geometry, skew angles, and laser drilling effects etc on TMF crack initiation and propagation.
Comparison of smooth specimen data with results obtained on the specimens with small holes allows assessment of the TMF endurance and component structural life of the notched structures as well as evaluation of the role that local stress concentration around small features produce. Thus, these TMF test results can be directly used to evaluate structural life of the cooled airfoils as well as provide necessary information on the applicability of smooth specimen TMF data to the assessment of real service components with small features causing local stress concentration.

This paper contains two major parts, namely the description of the novel experimental technique and cracks growth results shedding light on the mechanisms and kinetics of TMF in single crystals. The new experimental machinery reported in this paper are as follows; (i) notched test method and procedure for TMF crack growth; (ii) successful demonstration of induction thermograpghy for capturing crack growth verses cycle count and subsequent analysis of that data.; (iii) fast cycle thermomechanical fatigue testing using active cooling allowing 30 second heat up and 30 second cooling under sinusoidal command and feed back response.

Using this new experimental technique we show that (i) the life of TMF specimens with notched holes exhibit a 4 times debit compared to smooth gage section specimens under the same loading conditions. In addition (ii) we investigated the effect of the hole secondary crystallographic orientation on crack initiation and propagation. (iii) All tests demonstrated that the cracks start crystallographically along the <111> crystallographic plane and later change to mixed mode fracture. (iv) Fractographical analysis using both optical and SEM microscopes revealed that major crack propagation takes place at the low temperature portion of the cycle in the OP test, however there is noticeable damage accumulation during the high temperature compressive load portion of the cycle. And finally (v) crack propagation under TMF loading conditions is considerably faster than corresponding isothermal LCF crack growth tested at the temperature and similar loading conditions of the tensile part of the TMF cycle

The plan of the paper is as follows: in the next section we will describe the experimental set up and the testing methodology as well as the specific measurement techniques that have been used. In Section 3 some experimental results and TMF cracks will be discussed. We would also compare the TMF lifing results of "holed" specimens against smooth specimens data. The analysis of the fracture surfaces and the discussion of possible crack propagation mechanisms will be discussed in Section 4. We close with some concluding remarks.

2. TMF test set up

During the test, strain and temperature vary simultaneously therefore the total measured strain in a TMF test specimen is the algebraic sum of thermal strain and mechanical strain. These two components must be separated for measurement and control of the mechanical strain as follows; $\varepsilon_{mech} = \varepsilon_{total} - \varepsilon_{thermal}$. The test system compensates the thermal expansion effects on a dynamic basis so that cycling is accomplished with controlled values of mechanical strain applied to the specimen.

The temperature uniformity along the specimen was assessed under static temperature conditions. The measurements were taken at six locations within the gage section of the specimen; axially 0.33 inches apart at the top, middle and bottom; and radially 180° apart at the front and back as shown schematically in Figure 2. Using the measured temperatures as a guideline, adjustments were made to the coil position and diameter to ensure a temperature difference not greater than ±1% of the maximum temperature, expressed in Kelvin, occurred. Specimen temperatures were assessed at the peak temperature of each test using the Minolta Land Cyclops 100B infrared pyrometer.

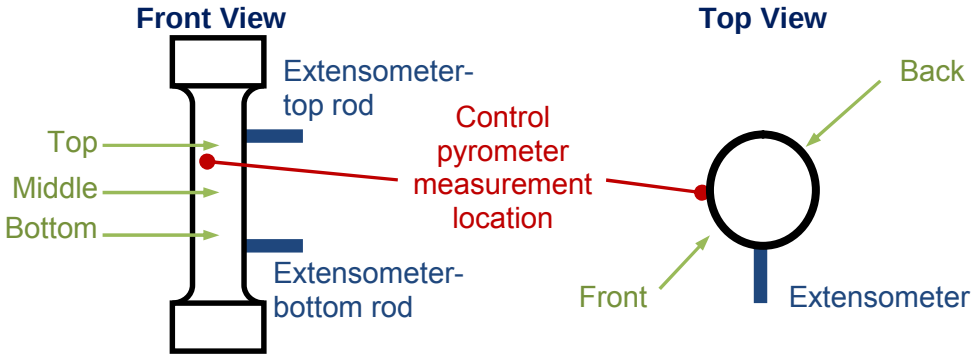

Figure 2 Schematic of temperature uniformity measurement locations (in green) on MT41 specimen

Specimen loading and instrumentation calibration were accomplished manually prior to transfer of control of the test machine to the computer system. The fully automated

computer control system was responsible for all facets of TMF testing including thermal strain calibration, test initiation, continuous or discontinuous cycling, and test termination. Special provisions were made to incorporate an optional high temperature dwell up to 30 minutes in each cycle. Data on specimen temperature, deflection, and load were measured and monitored continuously throughout the duration of the test. Tests were generally discontinued when load on the specimen decreased by 70 percent to prevent damage to the extensometer and possibly the heating system. Applicable ASTM standards were followed for performing specific parts of the TMF test[1].

The Minolta Land Cyclops 100B infrared pyrometer was used to periodically verify the specimen temperature during the test. The Spectrodyne disappearing filament pyrometer (DFP), model DFP2000, S/N DF20251, was used to calibrate the temperatures of both the Mikron and Minolta pyrometers prior to starting each test. The emissivity adjustment was performed at the maximum test temperature. During this calibration, the emissivity of the Mikron pyrometer was adjusted until the temperatures indicated by the DFP and the Mikron pyrometer matched.

One TMF test frame was used to generate the data. This frame consisted of a MTS, model 810, uniaxial servo-hydraulic test machine with a 22 kip (22,000 lbf) load capacity and the MTS 493.01 digital control system with MTS 793 system software. An MTS air-cooled high temperature axial extensometer, model 654.54.11F, with a 25 mm gage length was used to measure strain.

Heating of the specimen during the TMF test was provided by an Ameritherm induction heater (model NovaStar, 5 kW 50-485 kHz) with an induction coil that consisted of 6 turns. The induction coil was designed to minimize circumferential and axial temperature gradients throughout the TMF test specimens. The temperature was verified periodically using a Minolta Land Cyclops 100B infrared pyrometer (S/N: 12962071). Temperature feedback during the test was provided to the MTS 491.01 controller for closed-loop temperature control by a Mikron MI-GA5 (P/N 5857370, 250-2000°C) infrared pyrometer.

Specimen temperature is required to vary periodically in perfect synchronization with mechanical strain. Natural convection and conductive cooling approaches have generally proved to be insufficient to cool the specimen at the desired rate. Accordingly, forced air-cooling of the specimen via an air blast directed on the specimen surface and through the center of the specimen was employed. The operation of the air was computer controlled through an electric-to-pneumatic 4-20 mA closed loop operation with temperature feedback provided in the manner as the sample is heated. In the heat up portion on the cycle the error between the command and the feed back instrument, in this case the control pyrometer, will call for either heat or cooling. The operator could adjust the PID setting on the induction furnace and the air valves separatly to establish to correct command vs. feedback response to establish the desired cycle shape and rate respoinse. In this program temerature verses time and strain verses time are sinusoidal with a 60

[1] These include E606: Practice for Strain Controlled Fatigue Testing; E1012: Specimen and load train alignment; E220: Temperature calibration; and E 83: Extensometer calibration and use E2368 Standard Practice for Strain Controlled Thermomechanical Fatigue Testing.

second period. Once set, the automated computer system assumed full control of specimen heating and cooling processes during the test. Both internal and external cooling was provided by compressed air. The internal cooling was made through the grips, while the external cooling was applied through four diffusion nozzles which were placed around the upper portion of the TMF test specimen. The positions of the external nozzles could be adjusted to help attain the minimum thermal strain hysteresis between heating and cooling portions of the thermal cycle.

After TMF testing the specimens were inspected to document macroscopic fracture signatures and to identify crack initiation sites. Both longitudinal and transverse sections of the failed specimens were cut and prepared for metallographic analysis. We have recorded crack morphologies, crack length distributions, and microstructural changes in the single crystal superalloy.

In this work we focus on the experimental procedure to measure the TMF life of the specimens with two holes, to some extent emulating the effect of the cooling holes in the cooled airfoils. Standard MT-41 thin wall, hollow TMF specimens were fabricated from PWA 1484 alloy single crystal bar castings with <001> orientation. The specimen wall thickness is 0.05" (1.27 mm) and the gage length is 1" (25.4 mm). Such a choice of the TMF specimen guarantees almost uniform through wall temperature distribution during cooling and heating cycles. Two cooling holes separated by 135° of radial rotation were laser drilled through thickness in the mid-plane of each specimen as shown in Figure 3. The secondary crystallographic orientation of the holes were not controlled, however

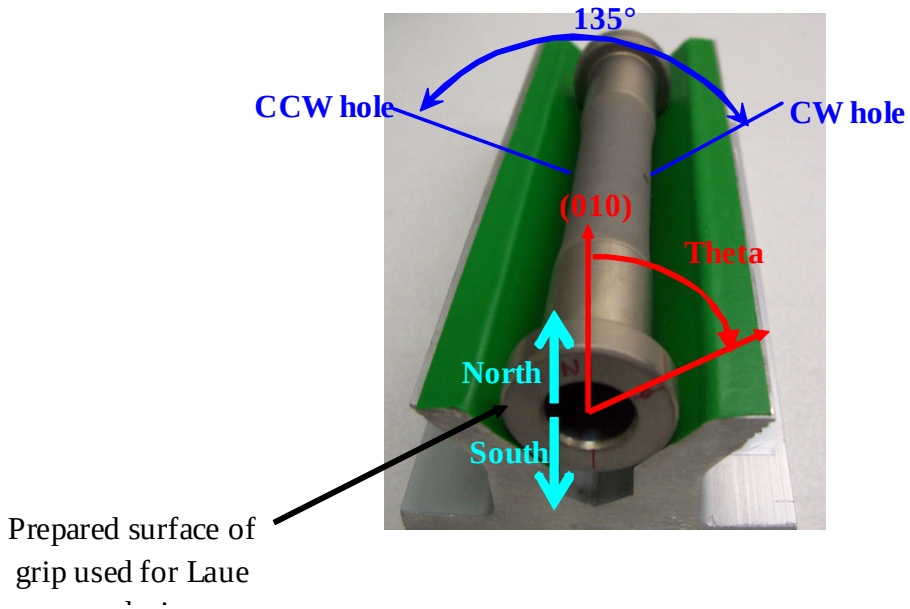

Figure 3. TMF specimen with two holes 135º apart. Also shown definition of the angles for Laue measurements on TMF specimens

Laue analysis of each specimen provides the information needed for the analysis of the secondary crystallographic orientation effects.

In the simplest case, for the primary orientation of <001> the first hole has orientation along <010> direction and the second hole is oriented along <110> crystallographic axis. Holes are situated far enough from each other, so the crack interaction effect is not observed until cracks reach significant (about the quarter of the circumference) length. Table 1 presents the results of the Laue investigation for some tested specimens. Here primary α represents the deviation of the specimen axial crystallographic axis from <001> and θ shows the deviation of one of the holes from <010> crystallographic axis.

Table I: Angles between the cooling hole locations and the <001 > poles

Serial Number	Primary Orientation	α	θ
19772A	001	7	7
19772B	001	5	77
19774A	001	3	64
19774B	001	4	59
19775B	001	4	60
19776A	001	1	71
19776B	001	1	29
19777A	001	5	43
19777B	001	6	38
19778A	001	3	15
19778B	001	4	22

Two infrared cameras, a FLIR SC3000 and a Jenoptik VarioCAM Hi-Res 640 were used to monitor crack growth around the holes in the gauge section of the TMF specimens.. Images were automatically acquired every 20 seconds throughout the TMF test and then post-test processed to quantify the crack progression. This system was originally co-developed between Pratt & Whitney and the National Research Center of Canada for early, non-contact crack detection and is called the Active Infrared Crack Detection system or AICD [18].

Due to the fact that the specimen heating is caused by Foucault currents any hole which causes the field disturbance may result in the overheating the area around the hole. We analyzed these regions using Infrared cameras. While the AICD process requires infrared images during each test, the actual emissivity is not required to determine the crack length. Therefore the infrared camera was not originally calibrated during this test program. Infrared and optical images taken during the heating portion for a typical specimen are presented in Figure 4. From the infrared image shown in this figure, the scale suggests that the temperature is significantly hotter in the hole. However from the optical image, there is no visual evidence of this temperature variation. Since the infrared image can only be affected by either temperature or emissivity, it would suggest that the emissivity is different for the hole compared to the bulk of the specimen. From Figure 4, an emissivity of 0.52 and 0.68 was determined for the specimen surface and hole respectively at the peak temperature of 1900°F during the 300 second hold. Assuming

that the emissivity is constant throughout the cycle, the emissivity can then be applied to each to determine the actual temperature. Using this corrected emissivity value there is no significant temperature variation between the bulk material, the crack, and the hole[2].

TMF specimens were tested using a fully reversed (R = -1), out-of-phase TMF cycle (i.e. the minimum strain occurred at the maximum temperature). Mechanical loading commenced during the heating portion of the thermal cycle and sinusoidal waveforms were used for both the strain and temperature cycles. The cycle time without dwell was 60 seconds, which consisted of 30 seconds of heating to the maximum temperature and then 30 seconds of cooling to the minimum temperature.

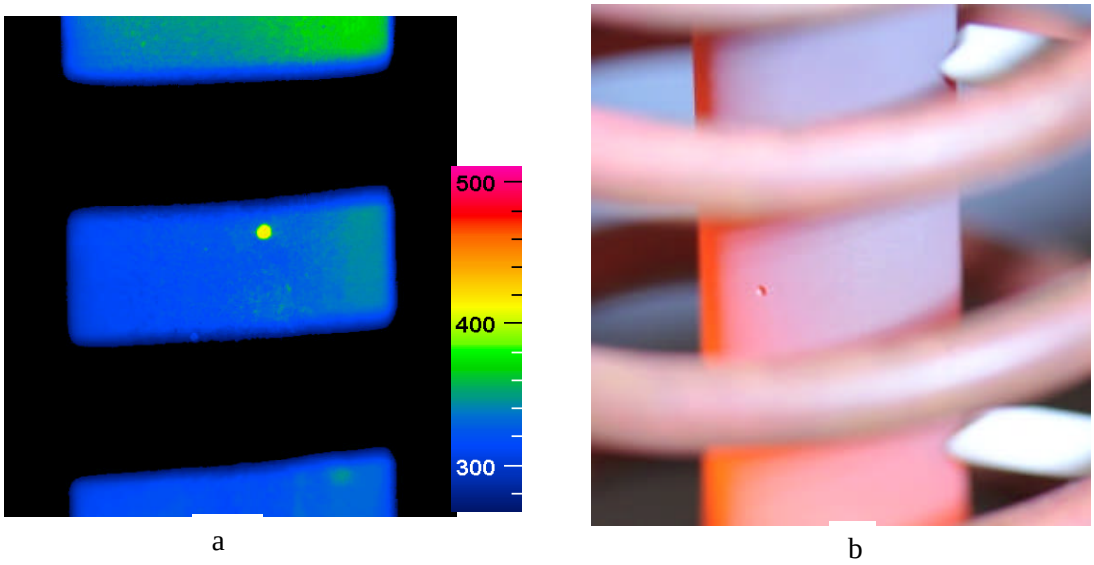

a b

Figure 4. Infrared image around the hole (a) and optical image of the same area

For this testing program, some specimens had a 300 second dwell at the peak (hottest) temperature during each TMF cycle. The test procedure is briefly described as follows. After a specimen was installed in the TMF test rig, the following sequence was performed:

1. Under zero force control, the specimen was heated to 1000°F and soaked for a period of one hour to develop a stable oxide layer on the specimen surface.
2. The specimen was then heated to the maximum target temperature of the test, either 1900°F, 2000°F, or 2100°F for the temperature calibration using the DFP.
3. The temperature dependent elastic modulus was measured at room temperature then at 100°F intervals between the minimum and maximum test temperatures. The modulus measurements were obtained under force control using a fully reversed sinusoidal waveform at 1 Hz and a stress range of approximately 10 ksi.
4. With the control system set to zero force (zero force control), the specimen was thermally cycled while adjustments were made to the cooling systems to minimize the thermal strain hysteresis.

[2] Our 2D thermal analysis also suggests that the temperature variation is not significant.

5. The temperature was verified at the maximum test temperature and final adjustments were made to the emissivity of the pyrometers used for the closed-loop temperature control and periodic temperature verification during testing.
6. The specimen was then cooled to room temperature and the room temperature strain was recorded.
7. The thermal strain history was recorded for the several cycles to ensure that a stabilized dynamic thermal strain response was attained. This thermal strain response was then used to account for thermal strain compensation.
8. The test was then switched to strain control and the thermal strain compensation function was verified by cycling the temperature while commanding and maintaining zero mechanical strain. The thermal strain compensation function was considered sufficiently accurate to commence a TMF test if the recorded force was smaller than 2% of the estimated maximum force for the TMF test.
9. Only after all the above steps, the actual TMF test was then started. The mechanical loading was initiated during the heating portion of the thermal cycle when the temperature corresponded to the zero mechanical strain.

3. Experimental Results

Twelve TMF tests have been completed on specimens with two holes (diameter 24 mils). In all tests cracks initiated at the holes and macroscopically propagated in the direction perpendicular to the maximum tensile stress. Initiation and propagation of TMF cracks from one of the holes is illustrated in the IR images shown in Figure 5. The specimen was tested at a maximum temperature of 1900°F and a total mechanical strain range of 0.5%. The images clearly show the formation of small cracks (Figure 5a)

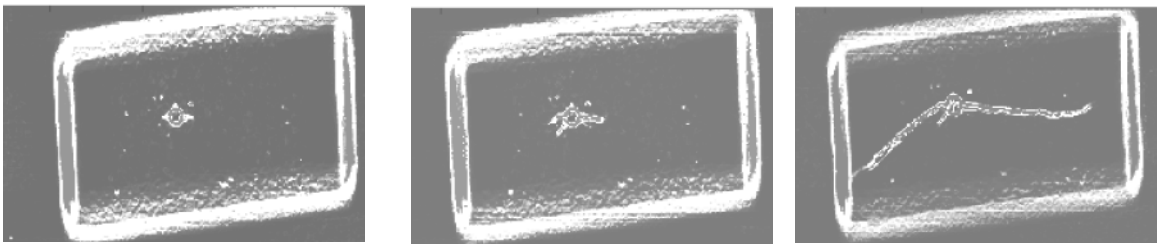

(a) (b) (c)

Figure 5: Infrared thermo-graphic images obtained from TMF specimen tested at a maximum temperature of 1900°F and a total strain range of 0.5%.

associated with the hole, and their progressive growth (Figure 5 b and c).

The results of OP TMF tests for the specimens with two holes are given in the Table 2.

Table 2. Results of the OP TMF tests for the specimens with two holes.

Serial Number	Temperature variation	Mechanical strain	N_f	Dwell (sec)
19774B	800 -1900F	0.5%	4612	0
19775B	800 -1900F	0.5%	7825	0
19778B	800-1900F	0.5%	3333	0
19777B	800 -1900F	0.8%	423	0
19778A	800 -1900F	0.8%	395	0
19772B	800 -2000F	0.5%	2803	0
19777A	800 -2000F	0.8%	301	0
19772A	800 -2100F	0.5%	1217	0
19776B	800 -2100F	0.8%	239	0
19776A	800-1900F	0.5%	1348	300
19774A	800-1900F	0.8%	191	300

Most of the tests were conducted without dwell time at high temperature. In order to estimate the dwell effects and to compare the results against test data obtained on smooth specimens we have conducted two tests with 5 minute dwell times. As one can see the 5 minutes dwell reduces the number of cycles to failure by about 3-5 times for tests at the $\pm 0.25\%$ of mechanical strain condition and in approximately 2 times for tests ran at $\pm 0.4\%$ of mechanical strain. Similar effects of dwell time were observed on the TMF tests of the smooth specimens.

The ratcheting (due to kinematic hardening) caused by inelastic effects is significant and slowly stabilizes after several hundred cycles. The shift of the stress-strain curves with cycle accumulation increases the maximum tensile stress at low temperature. Creep is suppressed at low temperature, and hence the major mode of energy dissipation becomes cracking. Thus, increasing the maximum value of tensile stresses with TMF cycles causes cracking at the low temperature regime. Hot compressive dwell (hold) noticeably increases the rate of ratcheting, since as the number of cycles increases the tensile stress at low temperature conditions becomes much larger and as a result the TMF life decreases.

We compare the test data above against results of similar TMF tests obtained on smooth specimens. Typical smooth specimen data is shown in Table 3.

Table 3. Some typical averaged results of the OP TMF tests for smooth specimens.

Temperature Range	Mechanical Strain	Dwell Time	N_f
800 -1900F	0.5%	0	10,000
800-1900F	0.5%	300	3,000
800 -1900F	0.8%	0	1,666
800 -1900F	0.8%	300	690

The average TMF life of smooth hollow specimens is approximately 2 to 4 times longer than life of the specimens with two small non-interacting holes under similar loading conditions. The difference increases with the increase of the strange range and slightly decreases with increase of the maximum temperature. It is important to note that the effect of dwell time is approximately the same in both smooth and holed specimen tests.

In order to evaluate the effect of the hole on the stress-state we developed an elastic visco-plastic model [5, 6] and implemented it into finite element software ANSYS as a USERMAT routine. The contours of Von Mises stress distribution due to OP TMF cycle is shown in Fig 6a. The hole causes localized stress concentration, which accelerates the TMF crack initiation. The stresses decay very rapidly as shown in Fig. 6b and do not affect the steady state crack propagation.

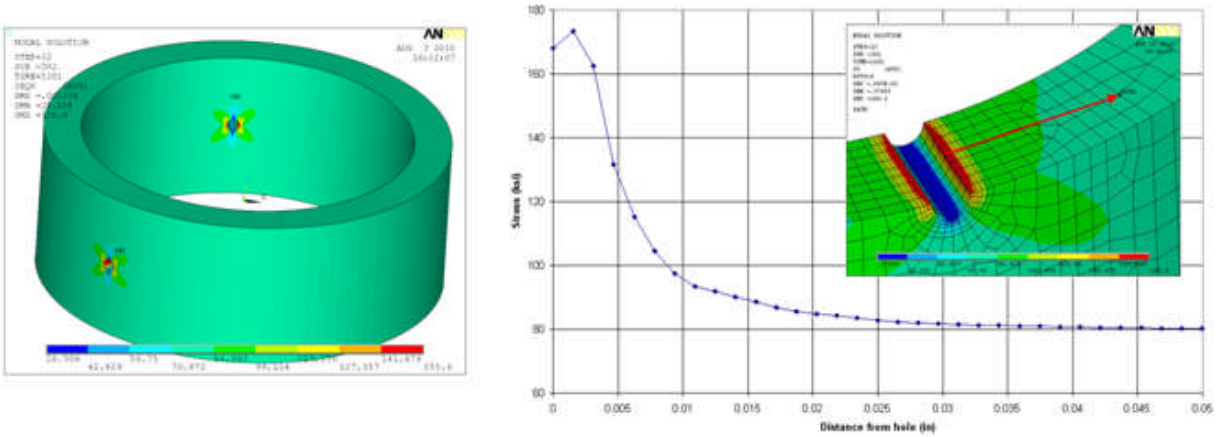

Figure 9. Elastic-visco-plastic model of TMF specimen. Stress distribution (a) and local stress distribution around the hole for 0.4% mechanical strain

With the increase of mechanical strain, the local stress level increases and might reach the yield at low temperature as it happens for example, during OP tests with temperature variation of 800F-1900F and mechanical strain magnitude of 0.4%. The typical stress-strain graphs for the near hole region and for the far field region are shown in Fig 10.

Model calculations using FRANC3Dng analysis at the low temperature end of the TMF cycle shows that the crack emanating from the hole oriented closer to <110> secondary crystallographic direction propagates faster than the crack emanating from the hole oriented close to <010> crystallographic direction. This is probably related to the difference in the stress levels as shown in Fig. 7. The difference in stress levels is caused by different yield properties along different crystallographic axes, which in turn causes differences in local stress and strain levels as well as the rate of ratcheting. To estimate the effect of the secondary crystallographic orientation we chose the specimen 19772A with the closest alignment (only 7 degrees apart) of the drilled holes to the <010> and <110> crystallographic axes. As one can see in Fig 8 the crack initiated at <110> oriented hole is the dominant one. As soon as one crack becomes significantly larger than the

second one the axisymmetric conditions are not valid anymore and the longest crack propagates faster.

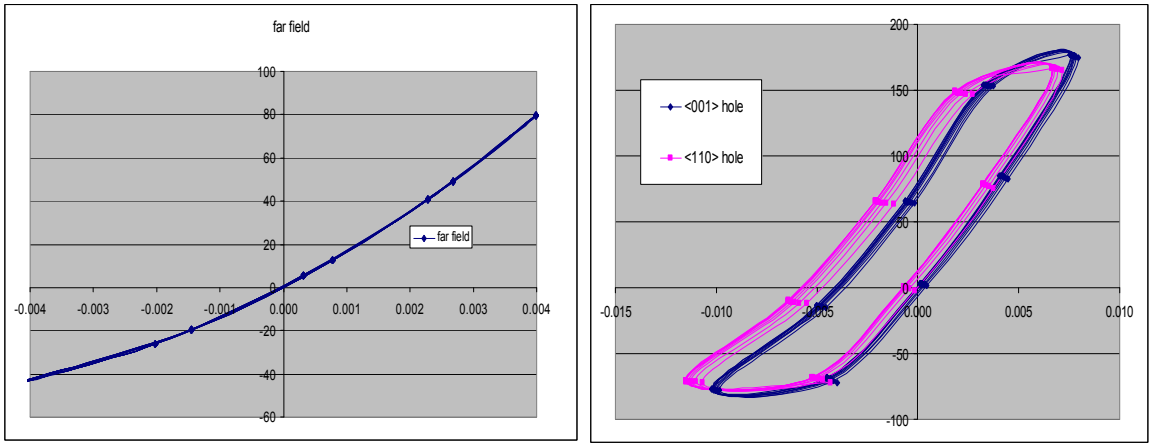

Figure 7. Stress-strain curves for OP TMF tests. Far field calculations (a) and stress-strain around holes (b).

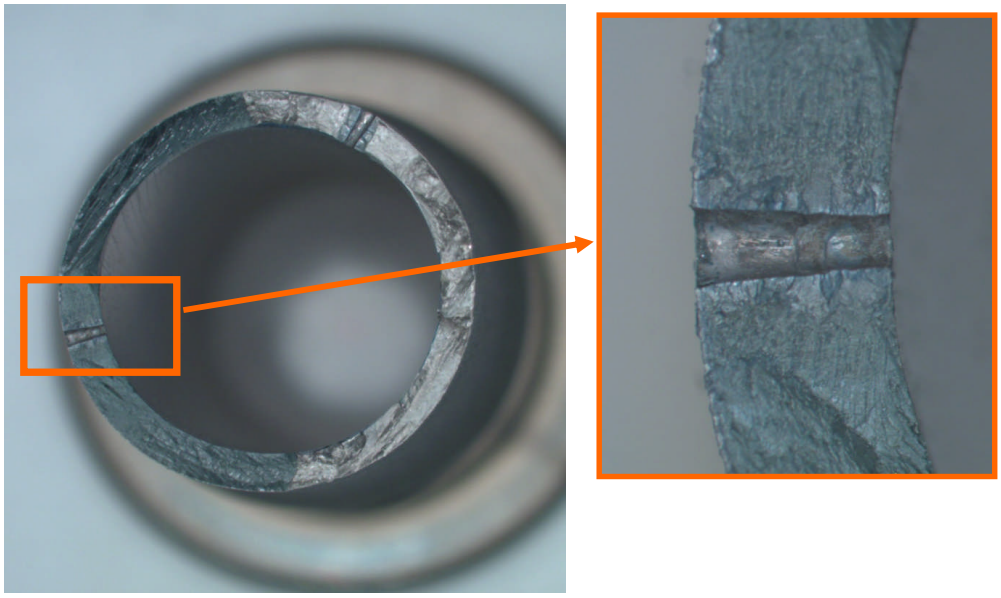

Figure 8. Fracture surface of the OP TMF crack(s) starting from the holes in the cylindrical specimens under mechanical strain range of 0.5% and temperature range of 800-2100F.

Cracks start propagating slowly and for most of the life time the acquisition system does not register any crack growth. Note that the initial crack length is taken as the diameter of the hole. Once crack initiation has occurred the crack growth rate increases very rapidly. With the increase of the maximum temperature of the TMF cycle the number of cycles to failure drops as can be seen from graphs in Fig 9.

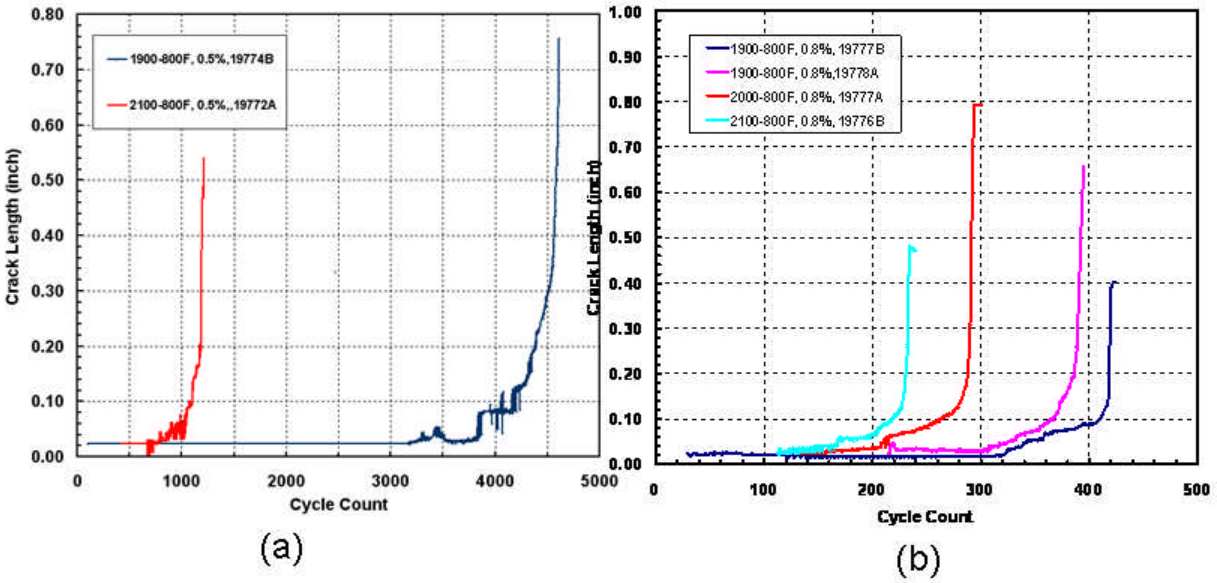

Figure 9. Dominant crack growth at 0.5% mechanical strain range (a) and 0.8% of mechanical strain range for different temperature ranges of OP TMF tests

Based on the FCG tests data shown in Fig. 9 we compare the crack propagation rate under TMF loading conditions against corresponding isothermal LCF crack growth tested at the temperature and similar loading conditions of the tensile part of the TMF cycle (or low temperature part which is the same for OP cycle) As one can see from the

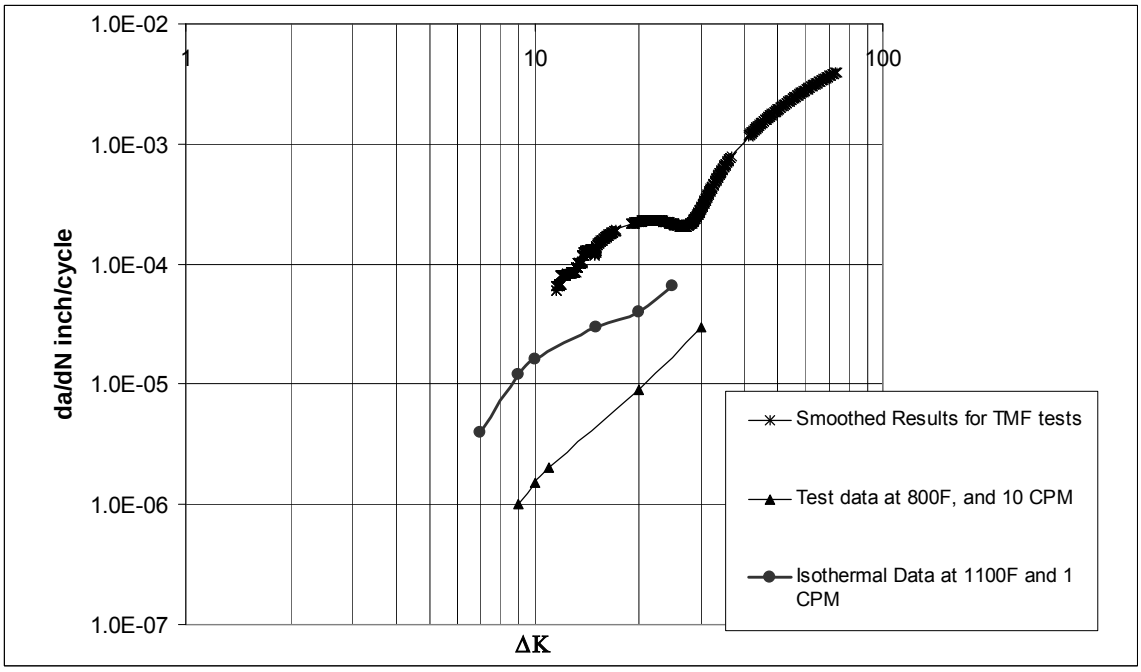

Figure 10. Comparison of crack growth rate during TMF tests against corresponding isothermal data

Figure 10, the TMF crack propagates considerably faster than corresponding crack during the isothermal low cycle fatigue tests. It means that at the high temperature portion of the cycle, the compressive visco-plastic deformations generate the damage which in turn reduces material crack resistance. The difference in the crack growth rate is noticable, so the damage tolerant design for TMF should account for TMF accelarating damage effects.

At low homologous temperatures, fatigue cracks propagate predominately along {111} crystallographic planes, and failure is driven by the shear mode. Examination of fracture surfaces reveals set of river marks that usually is attributed to coalescence of cleavage steps and is specific for brittle fracture. These steps are formed when different parts of the crack propagate on parallel crystallographic planes and are joined [11, 19] at the advancing crack front. Crack growth start from multiple nucleation sites along the hole. Micrographs of the tests demonstrate initial crystallographic crack propagations, which later changed to a non-crystallographic crack growth mode. The typical fracture surface is rather flat mode I failure with numerous small crystallographic facets. Crystallographic facets often create a chevron pattern as shown in Fig.11.

.

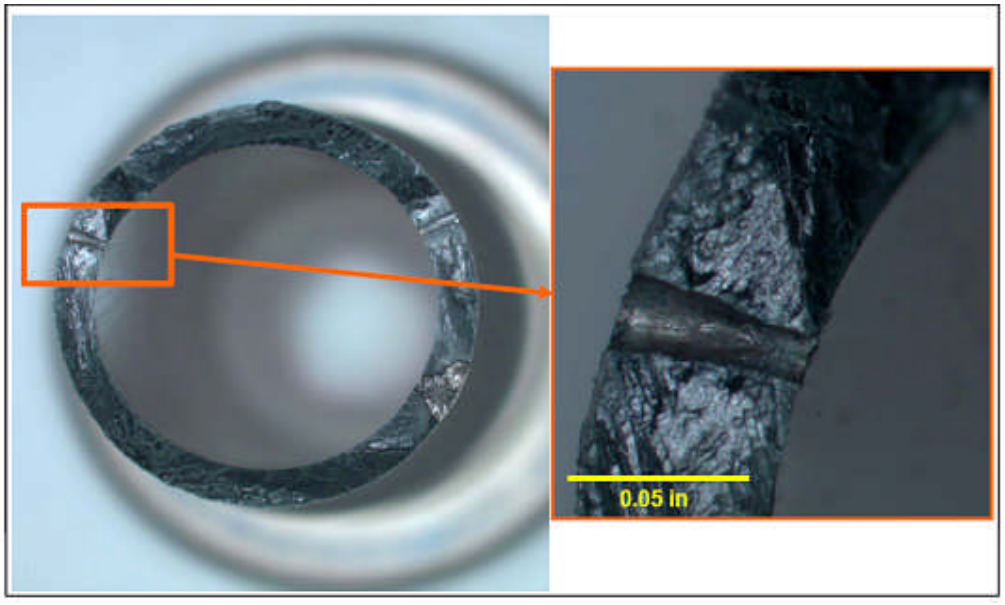

Figure 11. Crystallographic features including chevrons at the fracture surface after testing up to ε=0.8% at 800-1900F temperature range.

4. Fractographical analysis of TMF Crack Propagation

In order to analyze the micro-mechanisms of the TMF fracture we have conducted the SEM analysis of the fracture surfaces. We have performed the fractographical study of the four specimens fractured under different conditions as shown in Table 4. The goal

was to compare the damage mechanisms under different mechanical strain ranges, temperature ranges, as well as with and without hot dwell periods.

Table 4. Specimens chosen for SEM fractography.

Samples ID	Temperature variation	Mechanical Strain	Nf	Dwell	Max crack length [inch]
19774B	800-1900F	0.5%	4612	0	0.7556
19777B	800-1900F	0.8%	423	0	0.4022
19772A	800-2100F	0.5%	1217	0	0.5290
19776A	800-1900F	0.5%	1348	300	0.1617

The SEM pictures in Figure 12 show the TMF fracture surface of a specimen (19774B) tested at OP $\pm 0.25\%$ mechanical strain at 800F-1900F (426 C -1038 C) temperature cycle. The crack initiates along crystallographic plane and propagates in this mode for approximately 350 mm (13.8 mils). Then, due to the stress change caused by the crack growth and environmental enhancement, the crack surface shows crystallographic precipitate avoidance specific for high temperature and crystallographic cracks along two orientations normal to the crack surface. High magnification shows both coarse and fine cracking on multiple crystallographic planes with some indication of oxidation and precipitate avoidance. Mixture of the precipitate avoidance and matrix tearing along crystallographic steps indicate the damage progression at all temperature regimes: the steps formation at low temperature and high temperature deformation at high temperature. As one can see the SEM analysis suggests that crack propagation is the mix of crystallographic shear and Mode I separation processes.

Increasing of the high temperature cycle range to 2100F (1150 C) does not change the major cracking mechanisms. The specimen 19772A was tested at OP $\pm 0.25\%$ mechanical strain and temperature cycling between 800 F and 2100 F (426 C – 1150 C). The micrograph at Figure 13a shows that crack initiation takes place via a crystallographic mechanism, this time on multiple planes.

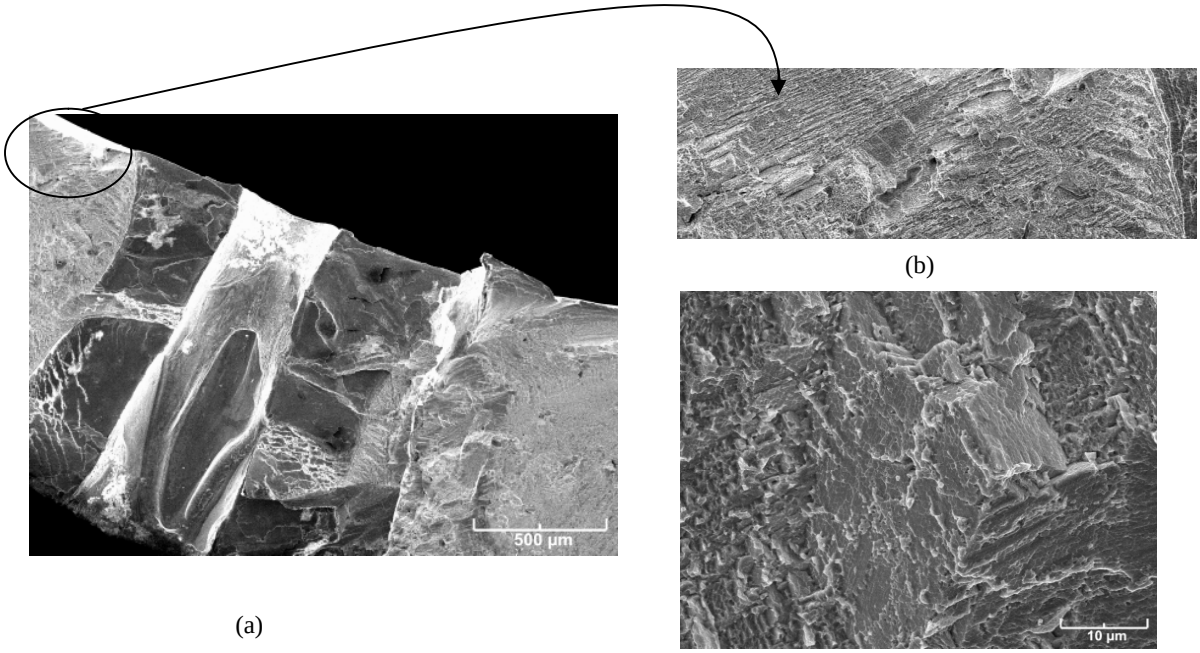

(a) (b) (c)

Figure 12. SEM pictures of TMF fracture surface of a specimen (19774B) tested at OP 0.25% mechanical strain magnitude and 426 C -1038 C (800 F-1900 F) temperature variation cycles. (a) next to the initial hole; (b) the details of transition region with deformation in two crystallographic orientation, and (c) the high magnification showing the cracking on multiple crystallographic planes.

Further, 'blocky' features illustrate striations with crystallographic steps and secondary cracks normal to the surface on the right portion of the micrograph, which is typical for environmental interaction.

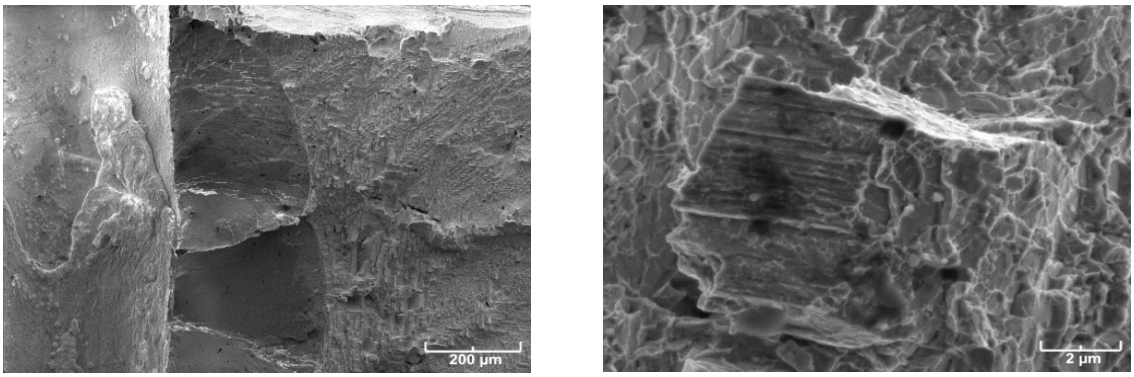

Figure 13. SEM pictures of TMF fracture surface of a specimen (19772A) tested at OP 0.25% mechanical strain magnitude and 426 C -1150 C (800 F-2100 F) temperature variation cycles. (a) next to the initial hole; (b) the details of facet with slip traces.

More detailed analysis shows cracking in the matrix and precipitate avoidance in many areas. Figure 13b illustrates precipitate fracture with matrix tearing. Also, the central region shows slip bands intersecting with crystallographic facet. Comparison with the fractography of the specimen (19776A) tested to $\pm 0.25\%$ mechanical strain at the 800 F

– 1900 F (426 C -1038 C) temperature range but with a 5 minute dwell at the high temperature regime clearly shows clear evidences of severe oxidation.

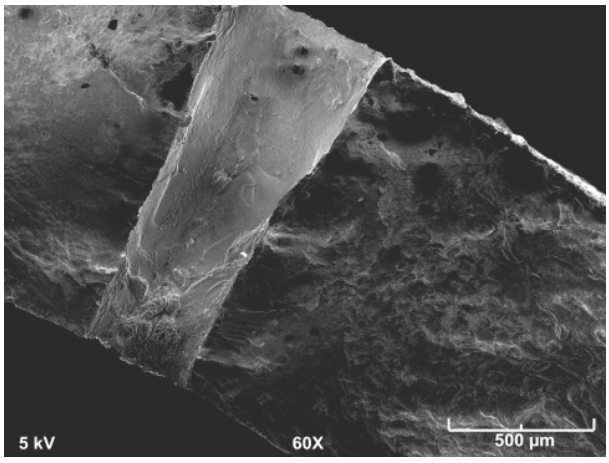

Figure 14. Crystallographic crack initiation and oxidized fracture surfaces after TMF testing with 5 minutes hot temperature dwell.

Nevertheless crack initiation at the hole has crystallographic characteristics as shown on the micrograph in Fig. 14.

We so far analyzed the fracture surfaces of TMF cracks initiated from the hole during the OP tests to $\pm 0.25\%$ mechanical strain at different temperature ranges, with and without dwell. The last example we present is the fractography of the specimen (19777B) tested to $\pm 0.4\%$ mechanical strain (see Table 2). Large mechanical strain range generates large stresses around the hole (see Fig. 10) and the crack propagates faster as can be seen from Fig. 11. As expected, the crystallographic modes of failure are more pronounced if high stress is applied. A similar pattern is observed even in dwell test results where environmental effects could prevent crystallographic fracture. In full accord to these observations the crack surface shown in Fig.15a demonstrates highly crystallographic growth with less time for oxidation and creep. A higher magnification shot illustrates that the fine slip bands intersecting the fracture surface. Similar results were observed by B. Lerch and S. Antolovich on Nimonic 80A Ni-based superalloy [20].

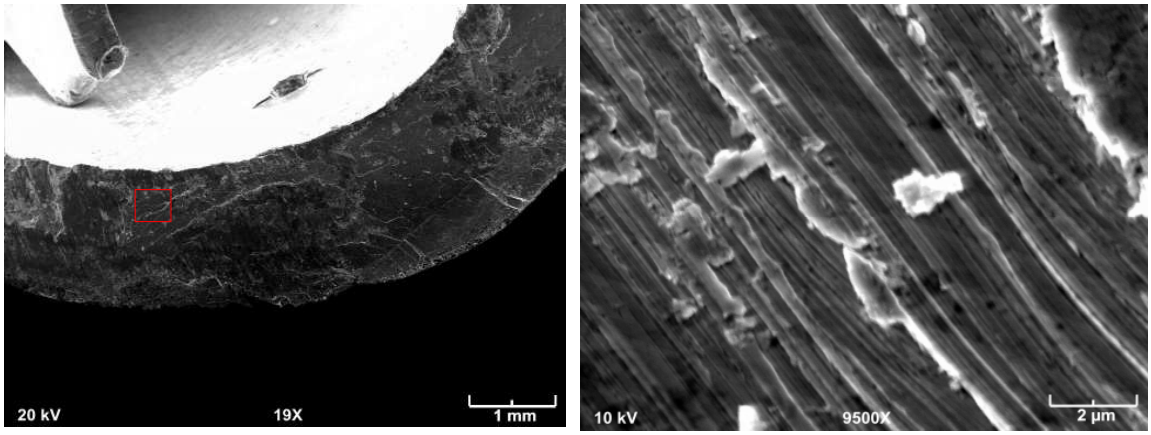

Figure 15. Fractography of the OP TMF specimen tested to $\pm 0.4\%$ mechanical strain. There are clearly evident large zones of crystallographic cracking (a) and fine slip bands in the selected area (b).

Based on these (and many similar ones, but not reported in this paper) observations, one can conclude that the cyrstallographic-type fracture occurs at the lower temperature since the precipitate are weak. At higher temperature in the TMF cycle the crystallographic

surfaces get oxidized and new surface tends to show precipitate avoidance, oxidation and some evidence of creep. At higher temperatures the cracking is usually in the interprecipitate areas with oxidation assistance and the lower temperature cracks or slip bands causing crack initiation in these regions. It is interesting to emphasize that the initiation from the hole appears to be in all cases crystallographic of nature. Comparative analysis of the initial TMF crystallographic cracking with crack length vs. cycle curves shows that after initial crystallographic cracking the crack growth rate slows down and it takes some time before the crack propagation continues in the second region. Important to notice that during the transition from crystallographic to mixed mode cracking, the crack direction is changed and aligned predominately perpendicular to the applied loading.

5. Concluding Remarks

In this paper we reported the crack growth results on test samples undergoing thermomechanical loading and showed that the life of TMF specimens with notched laser drilled holes exhibit a debit by as much as 4 times that of un-notched or smooth gage section specimens under the same loading conditions. Such a significant change in number of cycles to failure must be accounted in any damage tolerant design system. In addition we investigated the effect of secondary crystallographic oriented holes on each sample by drilling 2 holes 135° degrees apart from one another. We then discuss detailed fractographic analysis of the failed samples. All samples demonstrated that the cracks start crystallographically along the <111> crystallographic planes and later change to mixed mode I / crystallographic mode II fracture. Major crack propagation takes place at the low temperature portion of the cycle in the out of phase test, however there is noticeable damage accumulation during the high temperature compressive load portion of the cycle. This high temperature damage manifests itself, for example, as the precipitates avoidance on the micrographs as well as in the noticeable increase of the TMF crack growth rate. Crack propagation under TMF loading conditions is considerably faster than corresponding isothermal LCF crack growth tested at the temperature and similar loading conditions of the tensile part of the TMF cycle. In other words, an OP TMF test tested between the temperatures of 800 F to 1900 F has it's tensile loading at 800 F. Comparing the CGR of isothermal crack growth tests to the TMF shows significantly faster crack propagation for the TMF cycle. As results show, the applicability of the LEFM methods for single crystal TMF crack growth prediction is limited and at least should consist of mixed mode crack analysis.

A means of capturing real time CGR was needed. To accomplish this, a new method for detecting cracks during a TMF test using induction thermography was employed. This method, coined the Active Inferred Crack Detection System (AICD), was proven not only as a good way of finding cracks in-situ but also effective in following crack progression under cyclic loading conditions making it well suited to perform TMF crack growth testing. The method uses induction thermography and software co-developed by Pratt & Whitney and the National Research Center of Canada through a collaborative research agreement.

Acknowledgements

The authors are grateful for support and funding from the United States Air Force Research Laboratory through contract # FA8650-07-C-5252 and to Dr. Andrew Rosenberger for his support and attention to this work. Authors also would like to thank Prof. Stephen Antolovich and Dr. Venkat Seetharaman for the help with fractographical analysis and fruitful discussions.

6. References

1. Dame, T.L. "Anisotropic Constitute Model for Nickel Base Single Crystal Alloys: Development and Finite Element Implementation", PhD Thesis, University of Cincinnati, 1985.
2. DeLuca, D.P., Annis, C.G., Jr. "Fatigue in Single Crystal Nickel Superalloys", Office of Naval research (ONR) FR-23800, Aug. 1995
3. MacLachlan, D.W., and Knowles, D.M. "Creep-Behavior Modeling of Single-Crystal Superalloy CMSX-4", Metallurgical and Material Transactions, Vol. 31A, May 2000
4. MacLachlan, D.W., and Knowles, D.M. "The Effect of Material Behavior on the Analysis of Single Crystal Turbine Blades: Part II - Component Analysis", Fatigue Fracture Engineering Material Structures, Vol. 25, pp. 399-409, Nov. 2001.
5. Staroselsky A., Cassenti B.N., Combined rate-independent plasticity and creep model for single crystal *Mechanics of Materials* **42(**2010) 945-959
6. Staroselsky A., Cassenti B.N., On Creep, plasticity, and fatigue of single crystal superalloy. *Int. J. of Solids and Structures* **48**(2011) 2060–2075
7. Cowles, B. A. High cycle fatigue failure in aircraft gas turbines: an industry perspective. *Int. J. of Fracture*, **80**, pp. 147-163, 1996
8. Nissley, D.M., and Meyer, T.G. "Life Prediction and Constitutive Models fro Engine Hot Section Anisotropic Materials Program", NASA CR-189223, Sept. 1992.
9. Krutiy V., (2009) Sub-Modeling of Thermal Mechanical Fatigue Crack Propagation, MS Thesis, Rensselaer Polytechnic Institute.
10. N.K. Arakere ; S. Siddiqui ; F. Ebrahimi : Evolution of plasticity in notched Ni-based superalloy single crystals, *International Journal of Solids and Structures* **46** (2009) 3027 –3044
11. Cowles, B. A. High cycle fatigue failure in aircraft gas turbines: an industry perspective. *Int. J. of Fracture*, **80**, pp. 147-163, 1996
12. Zhou, H., Osawa, M., Harda, H., Yokokawa, T., Koizumi, Y., Kobayashi, T., Waki, M., Ro, Y., and Okada, I. "A Comparative Study of Thermo-mechanical Fatigue of Two Nickel Based Single Crystal Superalloys", Superalloys 2004, K. A. Green, et al. (eds.) TMS, Warrendale, PA, pp. 225-231, 2004

13. Zhang, Y.H., Withers, P.J., Fox, M.D., Knowles, D.M. “Damage Mechanisms of Coated Systems Under Thermomechanical Fatigue”, Materials Science and Technology, Vol. 15, pp. 1031-1037, Sept., 1999.

14. Bressers, J., Timm, J., Williams, S., Bennett, A., and Affeldt, E. “Effects of Cycle Type and Coating on the TMF Lives of Single Crystal Nickel Based Gas Turbine Blade Alloy”, ibid., pp. 56-67, 1996.

15. Meyer-Olbersleben, F., Goldschmidt, D., and Rezai-Aria, F. “Investigation of the Thermal Fatigue Behavior of Single Crystal Nickel Based Superalloys SRR 99 and CMSX-4”, Superalloys 1992, S. D. Antolovich, et al. (eds.) TMS, Warrendale, PA, pp. 785-794, 1992.

16. Wang, Y. C., Li, S.X., Zhou, L., Ai, S.H., Liu, F., Zhang, H., and Wang, G.Z. “Microstructures of a Single Crystal Nickel Based Superalloy After Thermo-Mechanical Fatigue”, Philosophical Magazine A, Vol. 84, pp. 3335-3351, 2004.

17. Chataigner, E. and Remy, L. “Thermo-Mechanical Fatigue Behavior of Coated and Bare Nickel Based Superalloy Single Crystals”, Thermo-Mechanical Fatigue Behavior of Materials, ASTM-STP 1263, M. J. Verrilli and M.G. Castelli (eds.), ASTM, West Conshohocken, PA, pp.3-26, 1996.

18. Genest M., Dudzinski D. C., Bulmer S., and Kersey R., Crack Detection Using Induction Thermography for Thermomechanical Fatigue Test AIP Conf. Proc. June 23, 2011, Volume 1335, pp 1727-1734 Review of Progress in Quantitative Nondestructive Evaluation: Volume 30A; doi:10.1063/1.3592137. Issue date 23 June 2011

19. Staroselsky A. Damage and cracking morphology in“*Advances in Fracture and Damage Assessment of Materials”*Ed.:**A**.Varvani-Farahani, and C.A. Brebbia, WITPress, UK, 2004

20. Lerch B. A. and S. D. Antolovich, (1990) Fatigue crack propagation behavior of a single crystalline superalloy, Metallurgical and Materials Trans. A, 21(8), pp.2169-2177